Available online at www.sciencedirect.com

SciVerse ScienceDirect

Ceramics International 38 (2012) 2065–2070

CERAMICS INTERNATIONAL

www.elsevier.com/locate/ceramint

Structural, thermal and electrical properties of Ti^{4+} substituted Bi_2O_3 solid systems

Gourav Singla, Paramjyot Kumar Jha, Jasmeet Kaur Gill, K. Singh *

School of Physics and Materials Science, Thapar University, Patiala 147004, India

Received 10 March 2011; received in revised form 15 October 2011; accepted 18 October 2011
Available online 23 October 2011

Abstract

In the present study, the effect of TiO_2 doping on $(1-x)$ Bi_2O_3 $(x)TiO_2$ ($x = 0.05$, 0.10, 0.15, 0.20) materials is investigated using X-ray diffraction (XRD), differential thermal analysis (DTA), ac conductivity, scanning electron microscopy (SEM) and energy dispersive spectroscopy (EDS). XRD results show the formation of single phase $Bi_{12}TiO_{20}$ at $x \geq 0.15$ concentration of TiO_2. It is observed that, the lower concentration of TiO_2 leads to the formation of mixed phase. The $x = 0.15$ and $x = 0.20$ samples exhibit regular and uniform distribution of the grains as compared to $x = 0.10$ sample. The highest conductivity is observed for $x = 0.15$ specimen, e.g., 9×10^{-7} S cm^{-1}.

Keywords: $Bi_{12}TiO_{20}$ phase; X-ray diffraction; Differential thermal analysis; Conductivity

1. Introduction

Bi_2O_3 has been studied extensively due to its application as sensors, solid electrolyte in fuel cells and high-temperature oxygen pumps [1,2]. Additionally, doped-Bi_2O_3 can also be used as a photorefractive material as well as low temperature co firing ceramic materials [3]. Bi_2O_3 exhibits different allotropes such as α, β, γ and δ phases. The highest ionic conductivity is reported in δ-phase of Bi_2O_3. This phase of Bi_2O_3 exhibits the conductivity of 1 S cm^{-1} between (600–800 °C) temperature ranges [4]. The δ-Bi_2O_3 exhibits fluorite type structure with space group $Fm\bar{3}m$. The presences of inherent oxygen vacancies are responsible for higher ionic conductivity in this structure. However, the ordering of these vacancies has also been reported in pure and doped Bi_2O_3 systems, which decrease the ionic conductivity [5–7]. Additionally, Bi segregation along the grain boundaries leads to decrease the ionic conductivity. Moreover, it is thermally stable in the narrow range of temperature (730–825 °C) [8]. Recently, efforts have been devoted to stabilize the highest conducting phase (δ-Bi_2O_3) at room temperature by doping of divalent to hexavalent dopant. The nature of dopant could be responsible to decide whether, it can work as an acceptor or donor for charge carriers [9]. Besides to ionic conductivity, photorefractive properties of these systems can also be modified by generating suitable defects in their crystal lattice. These defects can be created by selecting the appropriate dopant such as TiO_2. Basically, the substitution of TiO_2 may enhance the average grain size during sintering, which leads to higher electronic conductivity of the substituted system [10]. In addition to this, TiO_2 also acts as an active photocatalyst as reported by Linsebigler et al. [11]. However, the dopant concentration higher than the optimum value may lead to decrease conductivity due to defects ordering. So, it is worthwhile to study the effect of different concentration of TiO_2 in Bi_2O_3 on various properties. The objective of the present investigation is to determine the effect of TiO_2 doping on structural, thermal and ionic conductivity of Bi_2O_3 materials. The result of the as prepared samples is discussed in light of trapped oxygen vacancies and various phase formation.

2. Experimental

The oxides of Bi_2O_3 and TiO_2 were taken in appropriate stoichiometric amounts to prepare the composition of $(1-x)$ Bi_2O_3 (x) TiO_2 for $x = 0.05$, 0.10, 0.15, 0.20 by using standard solid reaction technique. The purity of the oxides was greater

* Corresponding author. Fax: +91 175 2393005.
E-mail address: kusingh@thapar.edu (K. Singh).

0272-8842/$36.00
doi:10.1016/j.ceramint.2011.10.043

than 99.9%. Appropriate quantities of the required constituent oxides of high-purity fine powders were thoroughly mixed in acetone for 2 h, using mortar and pestle and dried in the air. This mixture was heated at 700 °C for 4 h in the air using silica crucible and slowly cooled to room temperature. The calcined powder was reground and cold pressed after applying 10 ton pressure into pellets of 20 mm diameter and 2 mm thickness by adding poly vinyl alcohol as a binder. The green pellets were sintered at 800 °C for 12 h in the air followed by furnace cooling. The X-ray diffraction study of the sintered samples was done to identify crystalline phases. The X-ray diffractions of the samples were performed using PANalytical Xpert PRO with CuKα radiation (λ = 1.54 Å) obtained from the copper target using an inbuilt Ni filter. During XRD experiment, scan speed was 5°/min. Differential thermal analysis (DTA) was done to find out the phase transitions and stability of the samples. The DTA experiment was done with a heating rate of 10 °C/min from room temperature to 1000 °C in N_2 atmospheres. Gold sputtered pellets were used to carry out ac conductivity measurement in the temperature range of 100 to 700 °C. The two probe ac conductivity measurement was done using an ac impedance spectroscopy with Model 4274A multi-frequency Hewlett-Packard LCR meter in the frequency range of 0.1–100 kHz. The measurement is performed in the air by keeping the heating rate of 5 °C/min with temperature stability ±1 °C. The SEM and EDS were done on the fractured surface of the samples using JEOL JSM-6510 LV and INCA equipments, respectively.

3. Results and discussion

3.1. X-ray diffraction analysis (XRD)

The X-ray powder diffraction data were collected for all samples at room temperature between $20° \leq 2\theta \leq 70°$ at the scan speed of 5°/min. X-ray diffraction patterns of TiO_2 doped samples are shown in Fig. 1. All the four samples exhibited $Bi_{12}TiO_{20}$ cubic phase (space group 123) indexed with an ICDD card number (34-0097) along with the existence of α-Bi_2O_3 as impurity phase (ICDD card number 41-1449) in $x \leq 0.10$ samples (hypo-peritectic region). The formation of mixed phase for lower concentration of TiO_2 is also reported in the phase diagram given by Miyazawa [12]. X-ray diffraction patterns of the samples clearly show the increment in the volume fraction of $Bi_{12}TiO_{20}$ phases with increasing dopant concentration. The lower angle shifting in the XRD peaks, as shown in Fig. 2, are also observed in XRD patterns up to concentration of $x = 0.15$. This shifting is due to the strain induced because of the mismatch in the ionic radii of host cation Bi^{3+} (1.17 Å) and dopant cation Ti^{4+} (0.42 Å). The XRD results reveal that single $Bi_{12}TiO_{20}$ phase is formed above $x \geq 0.15$. On the other hand, the formation of tetragonal and rhombohedral phases have been reported when ZrO_2 ($Zr^{4+} = 0.73$ Å) and Gd_2O_3 ($Gd^{3+} = 0.94$ Å) are used as a dopant, respectively [13,14]. It is clearly shown that by reducing the average cationic radius of dopant lead to form $Bi_{12}TiO_{20}$ phase. In Fig. 3, the variation of lattice parameters of

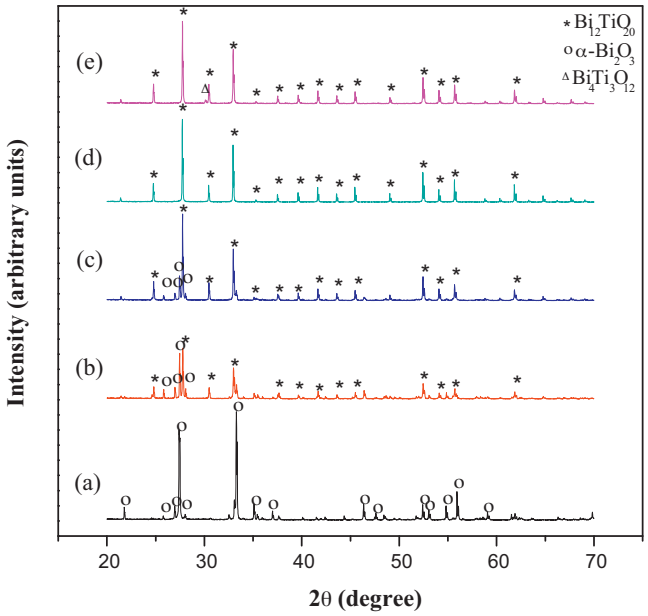

Fig. 1. X-ray diffraction patterns of $(Bi_2O_3)_{1-x}$ $(TiO_2)_x$ for (a) $x = 0$, (b) $x = 0.05$, (c) $x = 0.10$, (d) $x = 0.15$ and (e) $x = 0.20$ respectively.

$Bi_{12}TiO_{20}$ phase as a function of TiO_2 concentration is shown. As TiO_2 concentrations are increased, the lattice parameters increase for $x = 0.05$ to 0.15 samples. Maximum value is observed for $x = 0.15$ and then decreases for $x = 0.20$ sample. In the present samples, the lattice parameter calculation suggests that the solid solution limit lies at $x \geq 0.15$. It can be readily supported that the solid solution limit lies in the hypo-peritectic region. This non-linear relationship between the composition and the lattice parameter might arise due to the substitution of Bi^{3+} (1.17 Å) by smaller Ti^{4+} (0.42 Å) cation. Apart from this, incorporation of additional O^{2-} ions into the vacant sites might

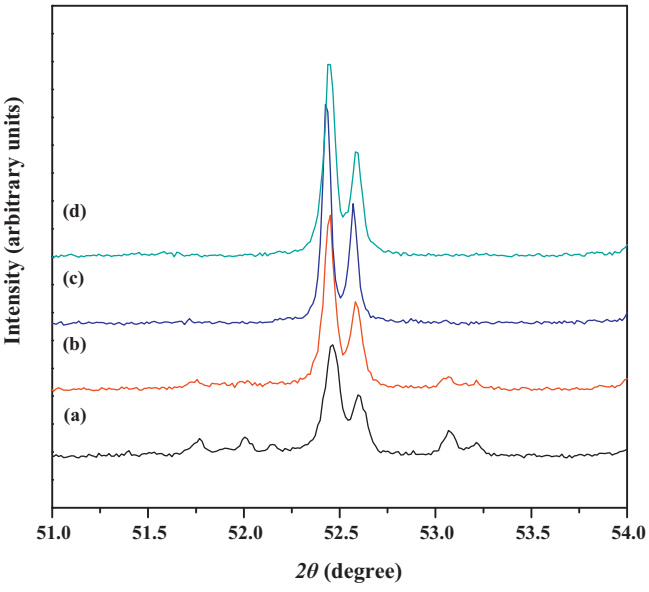

Fig. 2. Extended view of X-ray diffraction patterns of $(Bi_2O_3)_{1-x}(TiO_2)_x$ for (a) $x = 0.05$, (b) $x = 0.10$, (c) $x = 0.15$ and (d) $x = 0.20$ respectively showing diffraction angle shifting in peaks.

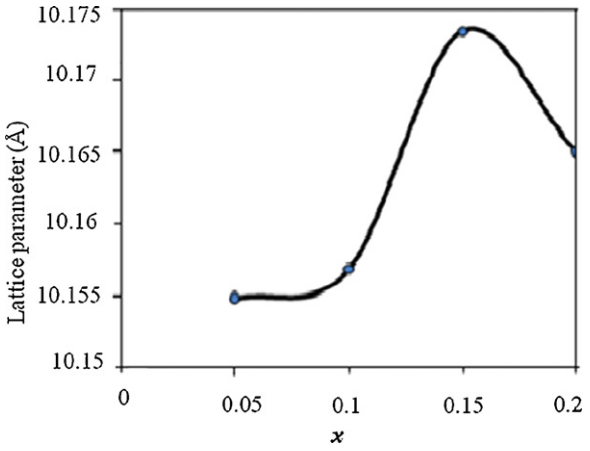

Fig. 3. Variation of lattice parameter with composition in $Bi_{2-x}TiO_{3+x/2}$.

be responsible to expand the unit cell as suggested by Abrahams et al. [14]. So, these two effects suggest that initially the variation in lattice parameter is due to the incorporation of O^{2-} ions in vacant sites. On the other hand, ionic radii effect is prominent at a higher concentration of dopant, i.e., $x \geq 0.15$. The small decrement in the lattice parameter for $x = 0.20$ sample might be attributed due to the existence of tetragonal $Bi_4Ti_3O_{12}$ phase as observed in XRD of $x = 0.20$ sample. Many researchers have been reported the formation of this phase at higher sintering temperature (above 800 °C) [12,15].

3.2. Thermal analysis

Fig. 4 shows differential thermal analysis traces for all compositions of $(1 - x)$ Bi_2O_3 (x) TiO_2 $(0.05 \leq x \leq 0.20)$. It is clear from Fig. 4 an exothermic peak appears at 640 °C for sample $x = 0.05$ in cooling cycle. This thermal event is associated with the transition of δ-phase to **β**-phase at about 640 °C. For dopant concentration of $x = 0.10$, similar exothermic heat effect is found at about 630 °C again showing the transition of δ-phase to β-phase. As indicated by the XRD results, the presence of α-Bi_2O_3 phase, in the $x = 0.05$ and $x = 0.10$ samples, is responsible for exothermic peaks in cooling cycle of these samples. The energy associated with these peaks decreases with increasing content of dopant in $x = 0.05$ and $x = 0.10$ samples. On the other hand, for higher dopant concentration, no recognizable heating effect is detected during the cooling cycle. This is confirmed the absence of β-Bi_2O_3 phase in these samples. The XRD pattern of these samples could not show the presence of impurity phase as indicate in Fig. 1(c) and (d). Similar results have been reported in various doped Bi_2O_3 samples [12,14,16,17].

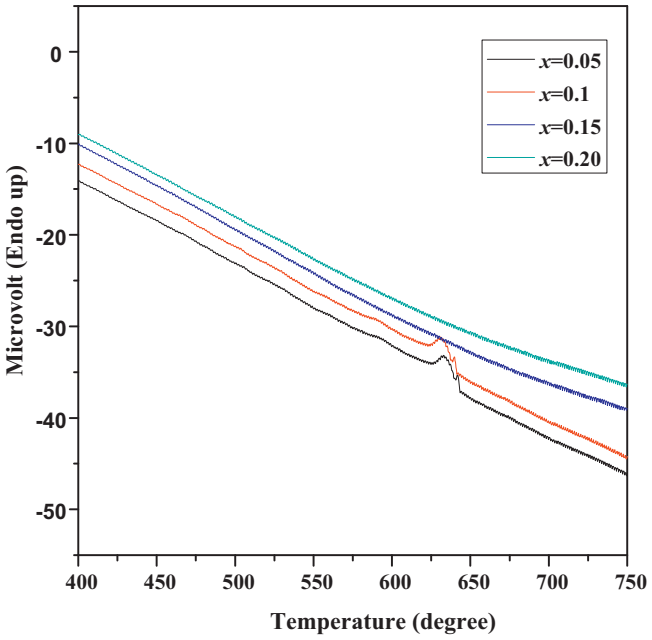

Fig. 4. DTA for $x = 0.05$, 0.1, 0.15 and 0.2 samples for cooling cycle.

3.3. Electrical conductivity analysis

Impedance spectroscopy was used to measure the electrical conductivity of the synthesized samples. Selected impedance spectra were recorded in the temperature range of 200–750 °C and in the frequency range from 0.1 to 100 kHz. A typical impedance spectrum is shown in Fig. 5 for $x = 0.20$ sample which is taken at 450 °C. With the increase in temperature from 200 °C to 750 °C the resistivity of the sample-to-electrode has greater influence on the overall sample resistivity. The bulk resistivity is equal to the sum of the grain and grain boundaries resistivity. Although, at a low-temperature Bi_2O_3 has a significant electronic contribution in total conductivity. It is presumed that, in pure Bi_2O_3, the high-temperature conductivity is mainly due to ion conduction. The Arrhenius plots of total conductivity for composition $(1 - x)$ Bi_2O_3 (x) TiO_2 ($x = 0.05$, 0.10, 0.15 and 0.20) are shown in Fig. 6. Each conductivity plot can be divided into two linear regions one at low temperatures, and one at high temperatures, especially for $x = 0.10$, $x = 0.15$ and $x = 0.20$ samples. The separation of these linear regions occurred at about 660 °C for $x = 0.15$ and 675 °C for $x = 0.20$

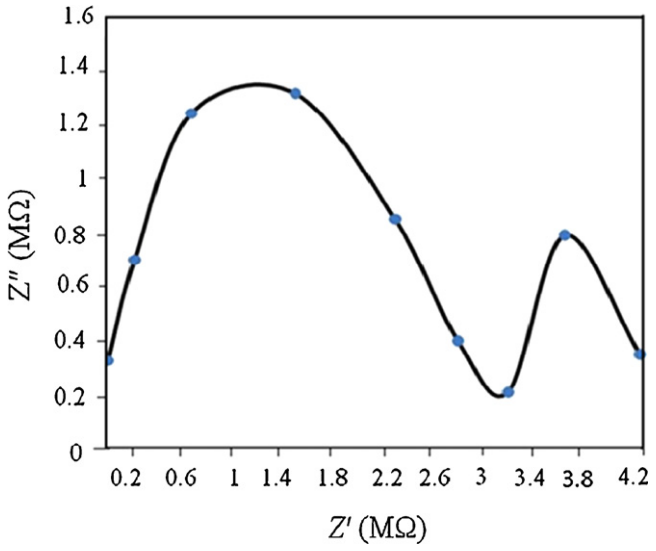

Fig. 5. Impedance spectrum of $x = 0.2$ sample at 450 °C.

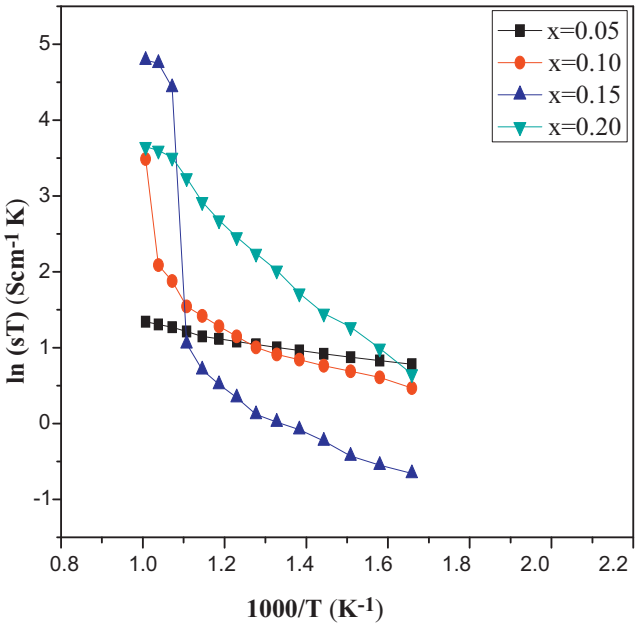

Fig. 6. Arrhenius plots of conductivity for $x = 0.05$, 0.10, 0.15 and 0.20 over cooling cycles.

samples. This discontinuity in conductivity curves has been attributed to small changes in oxygen stoichiometry in these samples. The conductivity data for all compositions are summarized in Table 1. The high-temperature conductivity, measured at 700 °C (σ_{700}), shows a drop in conductivity as compared to the literature value for the pure Bi_2O_3 system. Initially, conductivity increases with increasing content of TiO_2 and then decrease with increasing **TiO_2** content (2.7×10^{-7} S cm^{-1}) in $x = 0.20$ sample. The decrease in conductivity at the high temperature might be explained as a defect trapping effect [18]. It is well known that grain boundary effect is more prominent at the lower temperature than high temperature. Grain boundaries have an important effect on the overall conductivity. However, grain boundary is affected by the impurity level in the substituted system. The existence of the second phase, in the current study Bi_2O_3 phase in $x = 0.05$ and $x = 0.10$ samples affect the ionic conductivity because its segregation along the grain boundary during sintering [19–21]. The activation energy calculations in two different regions are also given in Table 1. The order of activation energy shows the ionic contribution in the present samples. Moreover, the higher values of activation energy might be explained because of more vacancy trapping at the higher temperature as compared to the lower temperature. In addition, various studies have shown that

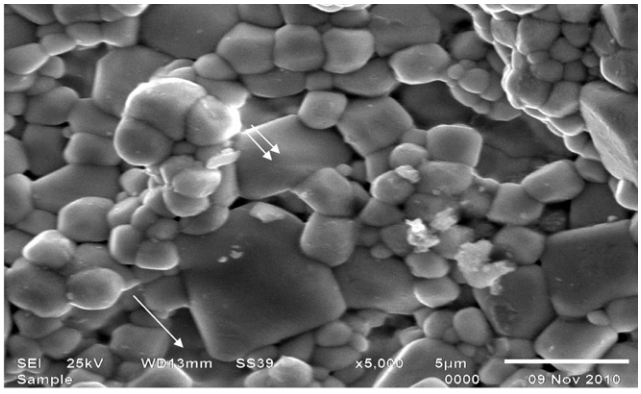

(a): SEM image for $x = 0.10$ at 5000X magnification.

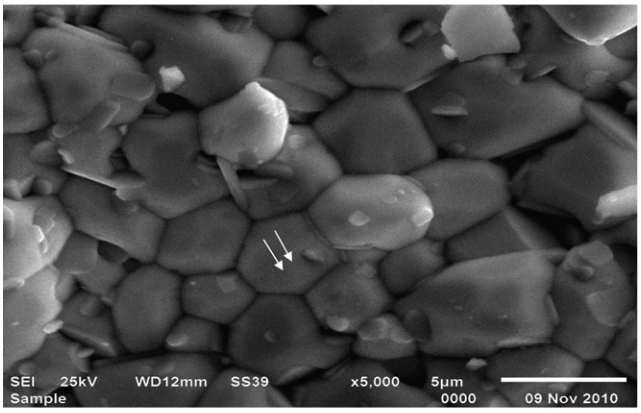

(b): SEM image for $x = 0.15$ at 5000X magnification

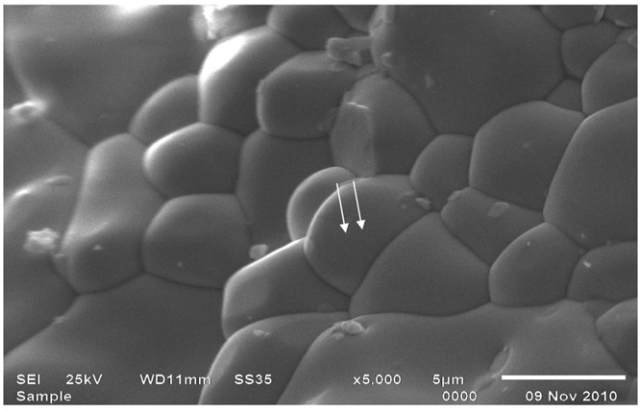

(c): SEM image for $x = 0.20$ at 5000X magnification.

Fig. 7. (a) SEM image for $x = 0.10$ at 5000× magnification. (b) SEM image for $x = 0.15$ at 5000× magnification. (c) SEM image for $x = 0.20$ at 5000× magnification.

Table 1
Conductivity parameter for composition in the $(Bi_2O_3)_{1-x}(TiO_2)_x$ system.

x	$\sigma_{300\ °C}$ (S cm^{-1})	E_a (eV) <450 °C	$\sigma_{650\ °C}$ (S cm^{-1})	E_a (eV) >650 °C
0.05	3.6×10^{-8}	0.92	3.8×10^{-8}	1.42
0.10	2.7×10^{-8}	0.98	7.0×10^{-8}	1.31
0.15	9×10^{-9}	1.043	9.0×10^{-7}	1.15
0.20	1.3×10^{-8}	0.95	2.6×10^{-7}	1.25

the presence of impurity suppresses grain growth, resulting in the small grain size and a larger grain boundary volume fraction. Therefore, these impurities provide a blocking layer within the grain boundary that makes the grain boundary less conductive and decreases the total conductivity. So, the presence of secondary phase such as Bi_2O_3 may affect the conductivity which decreases with increasing the dopant concentration. Since, at high-temperature grain boundary effect is less so the drop in conductivity observed at the high temperature must be due to defect trapping influence, which can be associated to the strong affinity of the oxygen vacancies with the small Ti^{4+} ions. Decrease in mobile oxygen vacancies and a subsequent drop in conductivity are expected because Ti ions are able to trap oxygen vacancy more effectively [18]. This is also consistent with the fact that the conductivities in cubic bismuth oxides are reduced due to the substitution of highly polarized bismuth ions with less polarized Ti^{4+} ions in the cation sub lattice [22]. Since the polarization is proportional to the cube of ionic radius of the constituent's cation [23]. So, the ionic conductivity of doped cubic bismuth oxide decreases with increasing dopant concentration of less polarized Ti^{4+}. The conductivity of the present sample is higher than earlier reported values of the same composition [24].

3.4. SEM and EDS analysis

The microstructure of fractured samples was further examined by SEM to correlate the results with X-ray diffraction. Fig. 7(a)–(c) shows the SEM micrographs of composition $x = 0.10$, 0.15 and 0.20, respectively. The SEM clearly shows the nonuniform distribution of the grains in the $x = 0.10$ sample. The EDS analysis of this sample shows the presence of two phases namely $Bi_{12}TiO_{20}$ and Bi_2O_3 phases as shown in Fig. 8 and Tables 2(a)–2(c). The distributions of the grains are very uniform and obvious, particularly in the $x = 0.15$ sample. It is observed that as the percentage of dopant increased the grain size is also increased as evident in Fig. 7(b) and (c). The addition of dopant increases the volume fraction of $Bi_{12}TiO_{20}$ phase. The $x = 0.15$ and $x = 0.20$ samples exhibit a further regular and uniform distribution of the grains as compared to $x = 0.10$ sample, which are clearly an indication of the presence of single phase. The EDS analysis of both samples was performed at least at four/five points to calculate the ratio

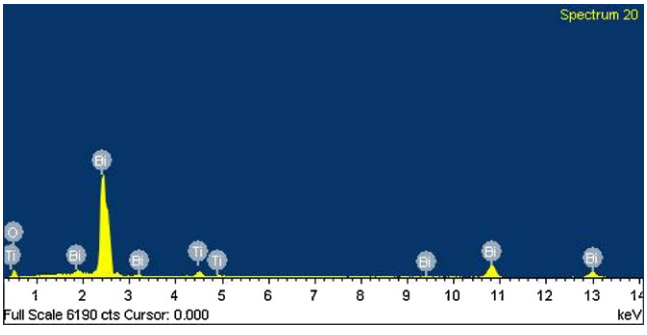

Fig. 8. Typical EDS analysis of $x = 0.10$ sample showing presence of $Bi_{12}TiO_{20}$ phase.

Table 2(a)
Results of EDS analysis of Bi and O as indicated by single arrow as indicated in Fig. 7(a).

Element	wt%	at%	Compd%	Formula
Bi	89.7	40.0	100.0	Bi_2O_3
O	10.3	60.0		
Totals	100.0			

Table 2(b)
Results of EDS analysis of Bi, Ti and O as indicated by double arrow as indicated in Fig. 7(b).

Element	wt%	at%	Compd%	Formula
Ti	1.6	2.9	2.7	TiO_2
Bi	87.2	36.4	97.3	Bi_2O_3
O	11.1	60.5		
Totals	100.0			

Table 2(c)
Results of EDS analysis of Bi, Ti and O as indicated by double arrow as indicated in Fig. 7(c).

Element	wt%	at%	Compd%	Formula
Ti	1.5	2.8	2.6	TiO_2
Bi	87.3	36.5	97.3	Bi_2O_3
O	11.0	60.5		
Totals	100.0			

of Bi/O, Ti/O and Bi/Ti. The atomic ratio shows the single $Bi_{12}TiO_{20}$ phase formation in both the samples (as evident in Tables 2(b) and 2(c). The conductivity of sample for $x = 0.10$ is on the lesser side than for $x = 0.15$ and $x = 0.20$ samples because of the presence of secondary phase in this sample. Similar results have been reported for cubic fluorite solid solutions [25].

4. Conclusion

The $Bi_{12}TiO_{20}$ single phase is formed at a higher concentration of dopant, e.g., $x = 0.15$ and $x = 0.20$ samples. The highest conductivity (9×10^{-7} S cm^{-1}) is observed for $x = 0.15$ sample, which is lower than pure δ-Bi_2O_3 phase. At high temperature, grain boundary effect is not prominent on conductivity. So, at the high temperature, the trapping of the oxygen vacancies by Ti^{4+} ions reduces the ionic conductivity in this system. Additionally, the formation of the tetragonal phase causes the reduction in oxygen anion hopping. The lower conductivity of the present samples can further be exploited as photo refractive materials.

Acknowledgements

Authors are very grateful to the University Grants Commission (UGC), New Delhi, India to provide the financial grant under vide letter no. 34-1 (Pun) SR dated 30/12/2008.

References

[1] I. Meatza, J.P. Chapman, F. Mauvy, I. Jose, R. Larramendi, I.M. Arriortua, T. Rojo, Novel composition above the limit of Bi:Zr solid solution; synthesis and physical properties of $Bi_{1.33}Zr_{0.67}O_{3+\delta}$, Mater. Res. Bull. 39 (2004) 1841–1847.

[2] A.A. Yaremcheko, V.V. Kharton, E.N. Naumovich, A.A. Tonoyan, V.V. Samokhval, Oxygen ionic transport in Bi_2O_3-based oxides: II. The Bi_2O_3–ZrO_2–Y_2O_3 and Bi_2O_3–Nb_2O_5–Ho_2O_3 solid solutions, J. Solid State Electrochem. 2 (1998) 308–314.

[3] M.H. Garrett, Properties of photorefractive nonstoichiometric bismuth silicon oxide, $Bi_xSiO_{1.5x+2}$, J. Opt. Soc. Am. B 8 (1991) 78–87.

[4] J.B. Goodenough, Oxide-ion electrolytes, Annu. Rev. Mater Res. 33 (2003) 91–128.

[5] B.D. Stojanovic, C.O. Paiva-Santos, M. Cilense, C. Jovalekic, Z.Z. Lazarevic, Structure study of $Bi_4Ti_3O_{12}$ produced via mechanochemically assisted synthesis, Mater. Res. Bull. 43 (2008) 1743–1753.

[6] G.H. Zhong, J.L. Wang, Z. Zeng, Ionic transport properties in doped δ-Bi_2O_3, J. Phys. Conf. Ser. 29 (2006) 106–109.

[7] D. Music, S. Konstantinidis, J.M. Schneider, Equilibrium structure of δ-Bi_2O_3 from first principles, J. Phys. Condens. Matter 21 (2009) 175403.

[8] Kapil Sood, K. Singh, O.P. Pandey, Synthesis and characterization of Bi-doped zirconia for solid electrolyte, Ionics 16 (2010) 549–554.

[9] V. Marinova, S.H. Lin, V. Sainov, M. Gospodinov, K.Y. Hsu, Light-induced properties of Ru-doped $Bi_{12}TiO_{20}$, J. Opt. A: Pure Appl. Opt. 5 (2003) 500–506.

[10] M.G.M. Sabri, B.Z. Azmi, Zahid Rizwan, M.K. Halimah, M. Hashim, M.H.M. Zaid, Effect of temperature treatment on the optical characterization of ZnO–Bi_2O_3–TiO_2 varistor ceramics, Int. J. Phys. Sci. 6 (6) (2011) 1388–1394.

[11] A.L. Linsebigler, G.Q. Lu, J.T. Yates, Photocatalysis on TiO_2 surfaces—principles, mechanisms, and selected results, Chem. Rev. 95 (1995) 735–758.

[12] S. Miyazawa, TSSG-pulling of sillenite $Bi_{12}TiO_{20}$ for EOS application, J. Korean Assoc. Cryst. Growth 9 (4) (1999) 424–431.

[13] S. Ekhelikar, G.K. Bichile, Synthesis and structural characterization of $(Bi_2O_3)_{1-x}$ $(Y_2O_3)_x$ and $(Bi_2O_3)_{1-x}$ $(Gd_2O_3)_x$ solid solutions, Bull. Mater. Sci. 27 (2004) 19–22.

[14] I. Abrahams, A.J. Bush, S.C.M. Chan, F. Krok, W. Wrobel, Stabilisation and characterisation of a new β_{III}-phase in Zr-doped Bi_2O_3, J. Mater. Chem. 11 (2001) 1715–1721.

[15] J. Zhou, Z. Zou, A.K. Ray, X.S. Zhao, Preparation and characterization of polycrystalline bismuth titanate $Bi_{12}TiO_{20}$ and its photocatalytic properties under visible light irradiation, Ind. Eng. Chem. Res. 46 (2007) 745–749.

[16] S. Yilmaz, O. Turkoglu, I. Belenli, Synthesis of β-phase $(Bi_2O_3)_{1-x}$(-$(Dy_2O_3)_x$ $(0.01 < x < 0.10)$ system and measurement of oxygen ionic conductivity, Res. Lett. Mater. Sci. 2007 (2007) 1–5.

[17] J.M. Amarilla, R.M. Rojas, A new family of bismuth-based oxide materials: $Bi_{2-2x}U_xLa_xO_{(3+3x/2)}$ $(0.333 \geq x \geq 0.038)$: synthesis, characterization, and phase transformations on aging, Chem. Mater. 8 (1996) 401–407.

[18] A. Kaiser, A.J. Feighery, D.P. Fagg, J.T.S. Irvine, Electrical characterization of highly titania doped YSZ, Ionics 4 (1998) 215–219.

[19] C. Tian, S.W. Chan, Ionic conductivities, sintering temperatures and microstructures of bulk ceramic CeO_2 doped with Y_2O_3, Solid State Ionics 134 (2000) 89–102.

[20] S.J. Hong, K. Mehta, Anil V. Virkar, Effect of microstructure and composition on ionic conductivity of rare-earth oxide-doped ceria, J. Electrochem. Soc. 145 (2) (1998) 638–647.

[21] B.C.H. Steele, Appraisal of $Ce_{1-y}Gd_yO_{2-y/2}$ electrolytes for IT-SOFC operation at 500 °C, Solid State Ionics 129 (2000) 95–110.

[22] D.S. Aidhy, S.B. Sinnott, E.D. Wachsman, S.R. Phillpot, Effect of ionic polarizability on oxygen diffusion in δ-Bi_2O_3 from atomistic simulation, Ionics 16 (2010) 297–303.

[23] W.D. Eric, S. Boyapati, N. Jiang, Effect of dopant polarizability on oxygen sublattice order in phase-stabilized cubic bismuth oxides, Ionics 7 (2001) 1–6.

[24] M. Valant, D. Suvorov, Processing, dielectric properties of sillenite compounds $Bi_{12}MO_{20-\delta}$ (M = Si, Ge, Ti, Pb, Mn, $B_{1/2}P_{1/2}$), J. Am. Ceram. Soc. 84 (12) (2001) 2900–2904.

[25] C.Y. Hsieh, K.Z. Fung, Crystal structure and electrical conductivity of cubic fluorite-based $(YO_{1.5})_x(WO_3)_{0.15}(BiO_{1.5})_{0.85-x}$ $(0 \leq x \leq 0.4)$ solid solutions, J. Solid State Electrochem. 13 (2009) 951–957.